Proceedings of the
Annual Stability Conference
Structural Stability Research Council
St. Louis, Missouri, April 16-20, 2013

Numerical and Experimental Investigation on the Post-Buckling Behavior, Ultimate Strength and DSM Design of Thin-Walled Cruciform Steel Columns

P.B. Dinis[1], P.S. Green[2], D. Camotim[1]

Abstract
This work reports on a numerical and experimental investigation concerning the buckling, post-buckling (elastic and elastic-plastic) and ultimate strength behavior of short-to-intermediate thin-walled equal-leg cruciform steel columns, as well as their Direct Strength Method (DSM) design. First, the main features of the column buckling and post-buckling behaviors are unveiled by means of GBT and ABAQUS shell finite element analyses (SFEA), evidencing the great similarities between the pin-ended (but with the end section secondary warping prevented) and fixed-ended column responses. Next, after revisiting an experimental investigation recently reported by Green (2012), the paper gathers a large column ultimate strength data bank comprising (i) a large number of numerical values, obtained from ABAQUS SFEA, and (ii) the experimental results available in the literature. The data bank, covering a wide column slenderness range, is then used to assess the quality of the estimates provided by the current DSM strength curves for the design against local, global and local-global interactive failures. On the basis of the above assessment, a novel DSM design approach is proposed, which leads to efficient (safe and accurate) ultimate strength predictions for the entire set of column failure loads considered in this work.

1. Introduction

Thin-walled cruciform columns are highly susceptible to torsional deformations since they exhibit no primary warping (the cross-section warping constant stems exclusively from secondary warping). Therefore, equal-leg cruciform columns with short-to-intermediate lengths buckle in pure torsional (global) modes that strongly resemble a combination of wall/plate outstand (local) buckling modes – it is virtually impossible to distinguish between local and torsional deformations. Since the column global and local buckling behaviors are associated with markedly different post-critical strength reserves, this distinction may have far-reaching implications on the development of an efficient (safe and economic) and rational (based on a sound structural model) design procedure for cruciform columns.

The buckling, post-buckling, strength and design of (equal-leg) cruciform columns have attracted the attention of a number of researchers in the past, namely Stowell (1951), Nishimo *et al.* (1968), McDermott (1969), Hutchinson & Budiansky (1974), Dabrowski (1988), Rasmussen & Hancock (1992), Chen & Trahair (1994) and, more recently, Makris (2003), Schurig & Bertram (2011), Dinis & Camotim

[1] Department of Civil Engineering and Architecture, ICIST, Instituto Superior Técnico, Technical University of Lisbon, Portugal. dinis@civil.ist.utl.pt and dcamotim@civil.ist.utl.pt
[2] Senior Civil Engineer, Bechtel Power Corporation, Frederick, MD, USA. pgreen2@bechtel.com

(2011, 2012), Trahair (2012, 2013) and Green (2012). As far as their design is concerned, some of these researchers devoted a fair amount of work to develop rules and procedures aimed at predicting the ultimate strength of short-to-intermediate columns, adopting mostly local buckling concepts. However, numerical simulations recently carried out by the authors (Dinis & Camotim 2011, 2012), concerning pin-ended and fixed-ended short-to-intermediate cruciform columns (i) shed new light on how to characterize and/or distinguish local and global (torsional) buckling, (ii) unveiled some surprising behavioral features, and (iii) concluded that the column design should be based on genuine torsional buckling concepts, instead of local buckling ones – this conclusion was recently confirmed analytically by Trahair (2012). Moreover, recall that the cruciform column torsional collapses are much more akin to plate outstand (local) failures than to the "traditional" column flexural and/or flexural-torsional collapses.

The aim of this work is to present numerical and experimental results concerning the buckling, post-buckling, strength and design of pin-ended ("cylindrical hinges" – end section secondary warping and one-axis flexural rotations prevented) and fixed-ended short-to-intermediate equal-leg cruciform columns. After showing some illustrative numerical results concerning the buckling, elastic-plastic post-buckling and ultimate strength behavior of such columns (Dinis & Camotim 2011, 2012), the paper presents column failure load data covering a wide slenderness range, obtained from (i) numerical simulations presented in this work, (ii) an experimental investigation carried out by Green (2012), which is revisited here, and (iii) experimental column ultimate strength values that have been reported in the literature. The numerical values are obtained through ABAQUS (Simulia 2008) shell finite element analyses (SFEA), adopting (i) fine 4-node isoparametric element meshes (length-to-width ratios close to 1) to discretize the columns, (ii) rigid plates attached to the end section centroids to model the supports and (iii) a linear-elastic/perfectly-plastic stress-strain curve to simulate the steel material behavior (residual stresses are disregarded). As for the experimental investigation, it involves nine cruciform columns with short-to-intermediate lengths and made of high-performance steel – the results presented comprise the column geometries, initial imperfections, material properties, failure loads and load vs. axial shortening equilibrium paths. The output of this effort is the collection of 31 experimental and 262 numerical failure loads, concerning columns with pinned and fixed end supports and various cross-section dimensions, lengths and yield stresses. This column failure load "data bank" is then used to assess the quality of their estimates provided by the current Direct Strength Method (DSM – *e.g.*, Schafer 2008) strength curves, concerning the design against local, global and local-global interactive failures. On the basis of the conclusions drawn from the above assessment, a novel DSM design approach is proposed and shown to lead to efficient ultimate strength predictions for the set of column failure loads considered in this work.

2. Buckling and Post-Buckling Behavior

The main results of a recent investigation (Dinis & Camotim 2011, 2012) on the buckling, post-buckling and ultimate strength behavior of thin-walled steel (E=210GPa, ν=0.3) cruciform columns are presented and discussed. The columns analyzed exhibit (i) pinned (warping prevented – P condition) and fixed (F condition) end sections, (ii) equal legs (80×4 mm), (iii) short-to-intermediate lengths and (iv) four yield-to-critical stress ratios – the elastic behavior may be viewed as associated with $f_y = \infty$.

2.1 Buckling Behavior

Figs. 1(a)-(b) show (i) the variation of the (GBT-based) critical load P_{cr} with the column length L (logarithmic scale), for P and F cruciform columns, and (ii) the buckled mid-span cross-sections of the pin-ended columns with L=20, 200, 1000 cm. These buckling results prompt the following remarks:

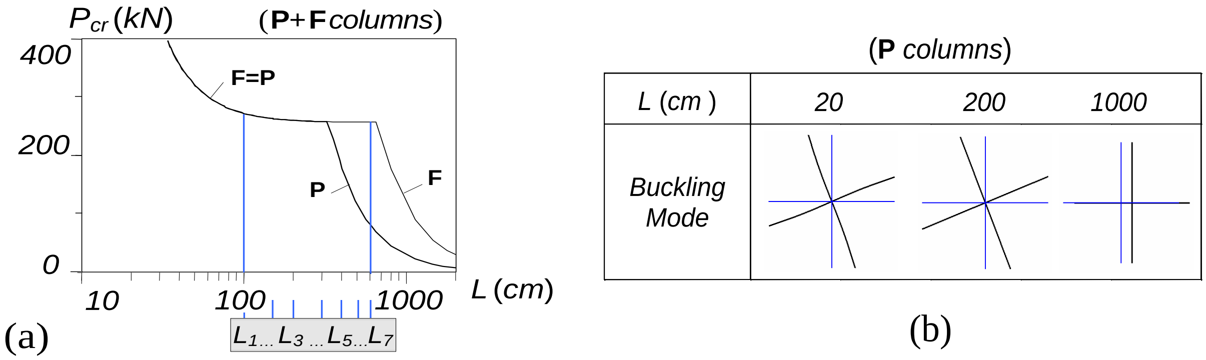

Figure 1: Pinned and fixed columns (a) P_{cr} vs. L curves and (b) three pinned column buckling mode shapes.

(i) The P_{cr} *vs.* L curve plateaus correspond to pure torsional buckling and the short-to-intermediate P columns only differ from their F counterparts in the smaller length range associated with the plateau, due to the flexural buckling load 75% drop – the F and P column torsional buckling behaviors are exactly the same. The transition from torsional to flexural buckling occurs for L=320 cm (P columns) and L=640 cm (F columns).

(ii) To investigate how the column post-buckling behavior varies along the P_{cr} *vs.* L curve plateaus, columns with lengths L_1-L_7=100; 150; 200; 300; 400; 500; 600 cm were selected: seven F columns (F_1-F_7 – 212.2≤f_{cr}≤200.9 MPa) and four P columns (P_1-P_4 columns – 212.2≤f_{cr}≤201.4 MPa).

2.2 Elastic Post-Buckling Behavior

Fig. 2(a) shows the upper parts of the post-buckling equilibrium paths P/P_{cr} *vs.* β (β is the mid-span cross-section rigid-body torsional rotation) of the P_1-P_4 and F_1-F_7 columns, all containing critical-mode initial

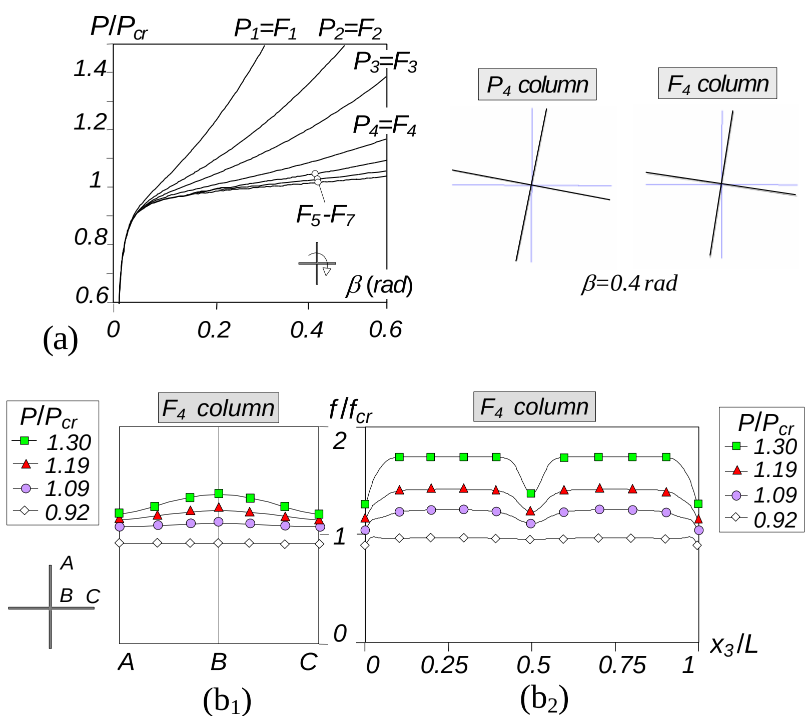

Figure 2: (a) P and F column P/P_{cr} *vs.* β paths, and P_4 and F_4 column buckled mid-span cross-sections; (b) longitudinal normal stress evolutions (b_1) at mid-span and (b_2) along the internal longitudinal edge (F_4 column and four load levels).

imperfections with small amplitudes (10% of the wall thickness $t = 4$ mm – torsional modes with mid-span rigid-body rotation $\beta_0 = 0.005$ rad) – also shown are the P_4 and F_4 column mid-span cross-section deformed configurations at $\beta = 0.4$ rad. Figs. 2(b_1)-(b_2) concern the F_4 column and provide the evolutions of the non-dimensional longitudinal normal stress distributions (f/f_{cr}) at mid-span and along the internal longitudinal edge. Observation of the results prompts the following comments:

(i) The P and F column post-buckling equilibrium paths, virtually identical for the same lengths, (i_1) are clearly stable (fairly high post-critical strength), (i_2) exhibit a post-critical stiffness that decreases with the column length, and (i_3) only involve cross-section rigid-body rotations.

(ii) Each cruciform F and P column behaves as the sum of four pinned-free (transversally) and fixed-ended or pin-ended (longitudinally) plates. This can be clearly confirmed by looking at the f/f_{cr} distributions shown in Fig. 2(b_1), concerning two adjacent legs of the F_4 column mid-span cross-section. Note that the stress distributions, also virtually identical for the F_4 and P_4 columns, (ii_1) become gradually "less uniform" as post-buckling progresses, with the higher value occurring at the corner, and (ii_2) exhibit a three half-wave longitudinal pattern, with lower values at the supports and mid-span, and higher values at the one-quarter and three-quarter-span cross-sections (see Fig. 2(b_2)). The mechanical grounds for the appearance and development of this three half-wave stress pattern stem from the axial extensions caused by the longitudinal variation of the torsional rotations (Stowell 1951, Rendall & Rasmussen 2012) – their values follow the torsional rotation slope/derivative.

2.3 Elastic-Plastic Post-Buckling Behavior

ABAQUS SFEA are again employed to investigate the elastic-plastic post-buckling behavior and failure of short-to-intermediate F and P cruciform columns exhibiting four yield-to-critical stress ratios ($f_y/f_{cr.av} \approx 1.2, 1.8, 2.6$ and ∞, corresponding to $f_y = 235, 355, 520$ MPa and elastic behavior – recall that $f_{cr.av} = 201$ MPa) – residual stresses are not taken into account. The results presented and discussed concern columns containing (i) critical-mode torsional (T) imperfections with amplitudes equal to 10% of the wall thickness t, or (ii) its combination with "non critical-mode" flexural imperfections (T+F), the latter with amplitude equal to $L/750$ (F columns) or $L/1000$ (P columns) – these amplitudes are in line with the average values measured in the thin-walled angle columns tested by Young (2004).

Figs. 3(a)-(b) show the upper parts ($P/P_{cr.av} > 0.5$) of five sets of equilibrium paths $P/P_{cr.av}$ *vs.* β and $P/P_{cr.av}$ *vs.* ε ($\varepsilon = \delta/L$ is the column axial extension, where δ is the axial shortening: average of the sums of the axial displacements at opposite nodes of the column end cross-sections), corresponding to the F_1,

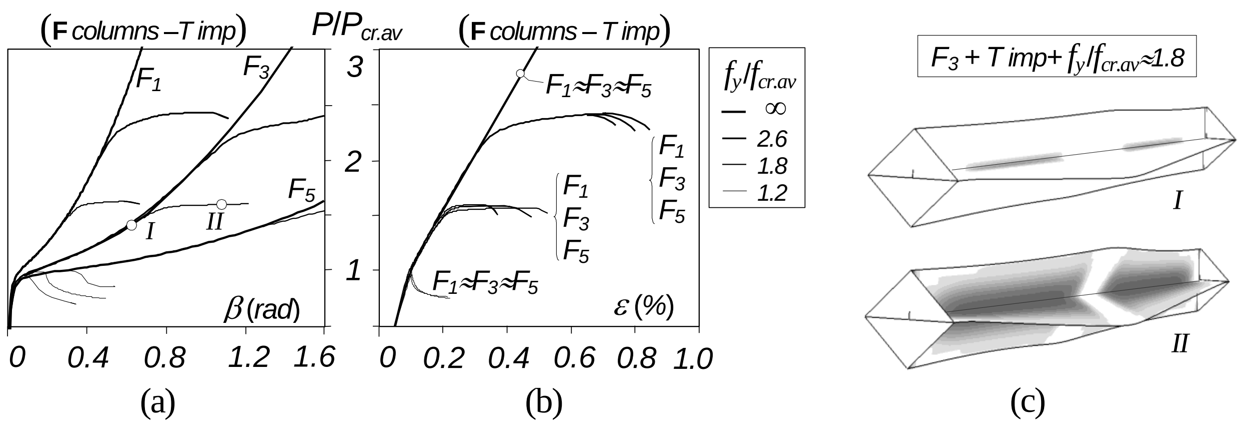

Figure 3: $P/P_{cr.av}$ (a) *vs.* β and (b) *vs.* ε paths (F_1, F_3, F_5 + 4 $f_y/f_{cr.av}$); (c) deformed shapes + plastic strains (F_3 + $f_y/f_{cr.av} \approx 1.8$).

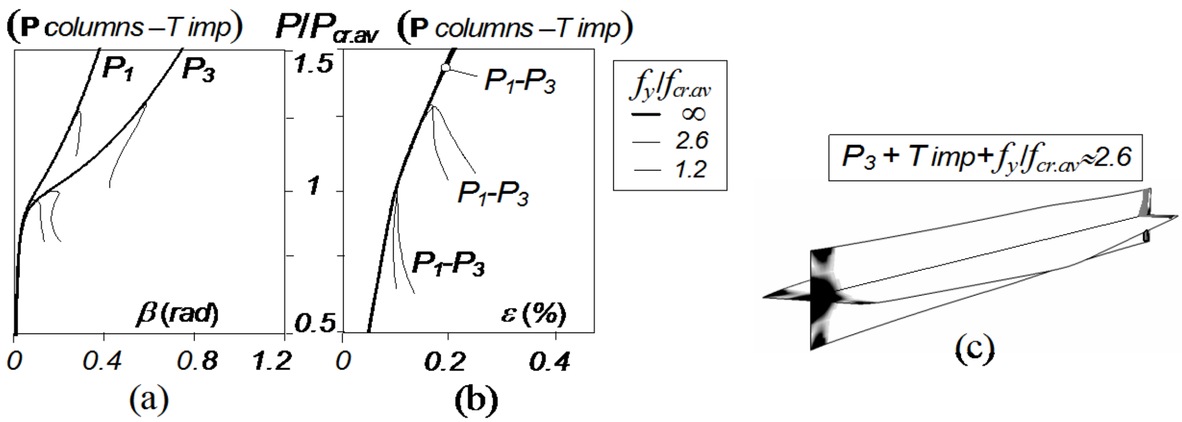

Figure 4: $P/P_{cr.av}$ (a) *vs.* β and (b) *vs.* ε paths (P_1, P_3 + 3 $f_y/f_{cr.av}$), (c) deformed shapes + plastic strains (P_3 + $f_y/f_{cr.av}\approx 2.6$).

Table 1: Variation of P_U with $f_y/f_{cr.av}$ and imperfection (F_1-F_7 + P_1-P_4 columns)

	P_U (kN)					
Column	f_y= 235 MPa		f_y= 355 MPa		f_y= 520 MPa	
	Imp		Imp		Imp	
	T	T+F	T	T+F	T	T+F
F_1	265.0	265.0	320.0	320.0	422.4	422.4
F_2	261.1	261.1	313.6	313.6	416.0	416.0
F_3	259.8	259.8	309.8	309.8	412.2	412.2
F_4	259.8	259.8	309.8	309.8	410.9	410.9
F_5	259.8	259.8	309.8	309.8	409.6	404.5
F_6	259.8	225.3	309.8	300.8	409.6	344.0
F_7	259.8	190.7	309.8	233.0	409.6	257.3
P_1	261.1	261.1	313.6	313.6	416.0	416.0
P_2	259.8	258.6	309.8	309.8	412.2	410.9
P_3	259.6	257.3	309.8	309.8	410.9	393.0
P_4	259.6	201.0	309.8	243.2	410.9	258.6

F_3 and F_5 columns with T imperfections. Fig. 3(c) concerns the F_3 column with $f_y/f_{cr}\approx 1.8$ and shows its deformed configuration and plastic strain distribution at the onset of collapse. Figs. 4(a)-(b) show similar equilibrium paths for the P_1 and P_3 columns (T imperfections), while Fig. 4(c) depicts the collapse mechanism of the P_3 column with $f_y/f_{cr}\approx 2.6$. Finally, Table 1 provides the variation of the P_1-P_4 and F_1-F_7 column ultimate loads (P_U) with the initial imperfection shape (T or T+F) for the given yield stress values. After observing these post-buckling results, the following conclusions can be drawn:

(i) The P and F columns with the same length and initial critical-mode (T) imperfections exhibit almost identical ultimate loads – indeed, restraining the end section one-axis flexural rotations increases the ultimate load by less than 2% for the shorter F_1 and P_1 columns. However, note that a previous investigation (Dinis & Camotim 2011) showed that this similarity does not extend to "perfectly pin-ended columns", whose end sections may warp freely – indeed, such columns exhibit much lower ultimate loads than their fixed-ended (and pin-ended, as unveiled in this work) counterparts.

(ii) Looking at Figs. 3(a)-(b), 4(a)-(b), and Table 1, one readily recognizes that the ultimate loads of the P_1-P_4 and F_1-F_7 columns with T imperfections remain practically constant as the (short-to-intermediate) length increases. This means that P_U is virtually unaffected by the amount of cross-section torsional rotation taking place before collapse – *e.g.*, note the huge difference between the collapse mid-span rotations concerning columns F_1 and F_5 (see Fig. 3(a)), while their ultimate loads are practically identical (see Fig. 3(b)). This means that failure is essentially governed by the normal stresses due to axial compression (basically the same for the F_1, F_3, and F_5 columns).

(iii) Diagram *I* in Fig. 3(c) shows that the onset of yielding occurs around the one-quarter and three-quarter span zones of the F_3 column internal longitudinal edge, where the normal and shear stresses, stemming from the torsional rotation slope/derivative, are higher (see Figs. 2(b)) – similar results were obtained for all columns with T imperfections. Collapse corresponds to the full or partial yielding of a relevant fraction of the column volume – diagram *II* in Fig. 3(c) shows that only the regions close to the end and mid-span cross-sections remain fully elastic at failure.

(iv) The onset of yielding occurs at the two end sections in all the P columns with T imperfections, where (iv_1) the longitudinal normal and shear stresses stemming from the torsional rotation slope are higher (*e.g.*, Stowell 1951) and (iv_2) non-negligible stress concentrations occur, due to the shell finite element modeling of the pinned supports (*e.g.*, Dinis & Camotim 2006). Collapse is then precipitated by the full yielding of both end sections, due to a combination of the above two factors and leading to the formation of "torsional plastic hinges". When the failure load is reached, practically the whole column volume is still in the elastic range – see the plastic strain distribution depicted in Fig. 4(c).

(v) The inclusion of a flexural component in the initial imperfection shape (*i.e.*, T+F imperfections) reduces the P_1-P_4 and F_1-F_7 column ultimate loads. This reduction (v_1) is minute for the shorter columns and (v_2) becomes progressively more sizeable as the length increases (higher susceptibility to torsional-flexural interaction) – it reaches 37% for the F_7 and P_4 columns with f_y=520 MPa.

3. Failure Load Data

Following the findings reported by (Dinis & Camotim 2011, 2012) which were summarized above, it was decided to assess the performance of the existing DSM design rules in predicting the failure load of thin-walled cruciform steel columns. The first step towards achieving this goal consists of putting together a fairly large column ultimate strength data bank comprising (i) numerical values obtained using the shell finite element model developed earlier, (ii) test results obtained from the experimental investigation recently reported by Green (2012) which will be revisited further later in this paper, and (iii) additional experimental values available in the literature.

3.1 Numerical Failure Loads

The numerical (SFEA) failure loads obtained concern the following thin-walled steel (E=210 GPa, ν=0.3) cruciform columns: (i) 224 fixed-ended columns, with cross-section dimensions 80×4 mm, 90×4 mm, 120×6 mm, 150×6 mm, 120×8 mm, and 150×8 mm, and (ii) 28 pin-ended columns, all with 80×4 mm cross-section. The column lengths were selected to ensure torsional critical buckling (*i.e.*, they fall within the P_{cr} vs. L curve plateaus – see Fig. 1(a)). For the F columns, their values are (i) 1000, 1500, 2000, 3000, 4000, 5000, 6000 mm (80×4 mm), (ii) 1500, 2000, 3000, 5000, 7000 mm (90×4 mm and 120×8 mm), and (iii) 2000, 3000, 5000, 7000, 9000 mm (120×6 mm, 150×6 mm and 150×8 mm). For the 80×4 mm P columns, the lengths are 1000, 1500, 2000, 3000 mm. In all analyses, residual stresses are disregarded and the steel constitutive behavior is modeled as elastic-perfectly plastic with various yield stresses: f_y=150, 235, 355, 520, 800, 1200, 1800 MPa – note that, to cover a wide critical torsional slenderness λ_T=$(f_y/f_{crT})^{0.5}$ range, several unrealistically high values are considered. Moreover, for all F and P columns, the adopted initial imperfections combine (i) a critical-mode torsional component, with an amplitude equal to 10% of the wall thickness t, and (ii) a non-critical-mode flexural component, with an amplitude equal to $L/750$ (F columns) or $L/1000$ (P columns) – *i.e.*, amplitudes in line with those measured by Young (2004) in thin-walled angle column specimens. All column dimensions, critical torsional (f_{crT}) and flexural (f_{crE}) buckling stresses, yield stresses and numerical ultimate stresses (f_U), and torsional (λ_T) and global (λ_E) slenderness are given in Appendices A (28 P columns) and B (224 F columns).

3.2 Overview of the Experimental Investigation at Lehigh (Green 2012)

This section presents an overview of the experimental investigation carried out at Lehigh University about two decades ago, but only recently reported by Green (2012). It involved cruciform columns made of high-performance steels, namely HSLA80 and HSLA100 grades – for comparison purposes, similar specimens made of ASTM A36 steel were also tested. The aim of the experimental program was to determine whether the then existing limits on local (plate) slenderness could be extended to cover high-performance steels whose yield stress exceeds 450 MPa. After briefly describing the test specimens, set-up and procedure, which includes providing the steel properties, specimen geometries and measured initial geometrical imperfections, the most relevant experimental results are displayed, namely equilibrium paths (load vs. axial shortening) and the corresponding ultimate loads and associated failure modes.

The test specimen fabrication and subsequent testing broadly followed McDermott's procedure (1969), even if a few changes were introduced – 1/2 inch plate (t=12.7 mm) was used to fabricate all specimens. While the A36 specimens (labeled as A) were flame cut, their HSLA80 and HSLA100 counterparts (labeled as B and C, respectively) were saw-cut. The individual plates/walls were welded together by means of double fillet weld pairs: 1/4 inch (6.35 mm) and 5/16 inch (7.94 mm), respectively for the A36 and HSLA specimens. The specimens had nominal leg widths (b) comprised between 1.5 and 4.5 inches (38.1 and 114.3 mm) and nominal lengths (L) ranging from 9 to 27 inches (228.6 to 685.8 mm). All member dimensions and steel yield stresses (f_y) are given in Table 2: (i) three specimens with 2b=3 inches (labeled A-3, B-3 and C-3), (ii) three specimens with 2b=6 inches (A-6, B-6 and C-6), and (iii) three specimens with 2b=9 inches (A-9, B-9 and C-9). Unlike the specimens tested by McDermott (1969), these were not stress relieved – instead, a unique procedure using a Whittemore gage to measure the residual stresses, that did not require any sectioning or utilizing any special strains gages, was used (Green 2012). Fig. 5(a) shows a typical measured residual stress pattern obtained for specimen B-6.

The specimens were instrumented with (i) ten strain gages, (ii) four string pots, and (iii) four linear variable differential transformers (LVDTs), as depicted in Fig. 5(b). Each specimen was carefully placed in the test machine (Baldwin Universal) and two gages, labeled "alignment", were used to check the specimen positioning (all legs had to be equally loaded). The remaining eight strain gages were placed in pairs on the mid-span opposite faces of each leg. The LVDTs and string pots were used to measure the mid-span deflections of each leg tip – while the LVDTs measured each leg tip transverse displacement (normal to the mid-line), associated with the cross-section torsional/local deformation, the string pots provided information about each tip longitudinal displacement, associated with the specimen axial shortening.

Initial geometrical imperfections were measured for each column specimen – the in-plane displacements of the four leg free (outer) longitudinal edges (δ_0 and w_0 – along the leg width and thickness, respectively) were surveyed prior to testing: measurements were taken at seven, nine, or eleven equally-spaced cross-sections along the specimens' 9, 18 or 27 inch length (*i.e.*, separated by $L/6$, $L/8$ or $L/10$ segments). Moreover, in order to assess the out-of-flatness of each leg, w_0 measurements were also taken along its inner longitudinal edge. The maximum measured δ_0 and w_0 values for each specimen (normalized w.r.t. the leg length L and width b, respectively) are given in Table 2 – each δ_0/L and w_0/L value corresponds to four (outer) and eight (inner and outer) longitudinal edges. Figs. 5(c)-(d) illustrate the above measurements and show the measured (i) sweep displacements δ_0 for specimen B-6 along the east and west edges, and (ii) out-of-flatness displacements w_0 for specimen A-6 along the north flange edge.

Three tension coupon tests were conducted for each specimen type to determine the steel material properties. For the high-performance steel specimens, the average yield stresses were (i) f_y=600 MPa for the HSLA80 specimens and (ii) f_y=758 MPa for the HSLA100 specimens. For the A36 specimens, the average tested yield stress was f_y=331 MPa. Concerning Young's modulus, the value published in the AISC/ANSI 360-10 Specification for Structural Steel Buildings (AISC 2010) is E=29000 ksi – the numerical results included in this work correspond to 200 GPa.

Table 2: Column specimen (i) geometries, (ii) coupon test yield stresses and corresponding squash loads, (iii) initial geometrical imperfection amplitudes (w_0 and δ_0) and (iv) experimental failure loads

Specimen	b (mm)	t (mm)	L (mm)	f_y (MPa)	P_y (kN)	δ_0/L	w_0/L	P_{Exp} (kN)	P_{Exp}/P_y
A-3	38.1	12.7	228.6	331	641	0.01133	0.00189	1013	1.65
B-3	38.1	12.7	228.6	600	1161	0.01333	0.00267	1324	1.19
C-3	38.1	12.7	228.6	758	1468	0.01333	0.00189	1612	1.15
A-6	76.2	12.7	457.2	331	1281	0.00383	0.00167	1571	1.24
B-6	76.2	12.7	457.2	600	2322	0.00500	0.00111	2647	1.15
C-6	76.2	12.7	457.2	758	2936	0.00867	0.00222	3103	1.07
A-9	114.3	12.7	685.8	331	1922	0.00444	0.00156	1821	0.95
B-9	114.3	12.7	685.8	600	3483	0.01148	0.00115	3704	1.07
C-9	114.3	12.7	685.8	758	4601	0.01259	0.00441	4572	1.04

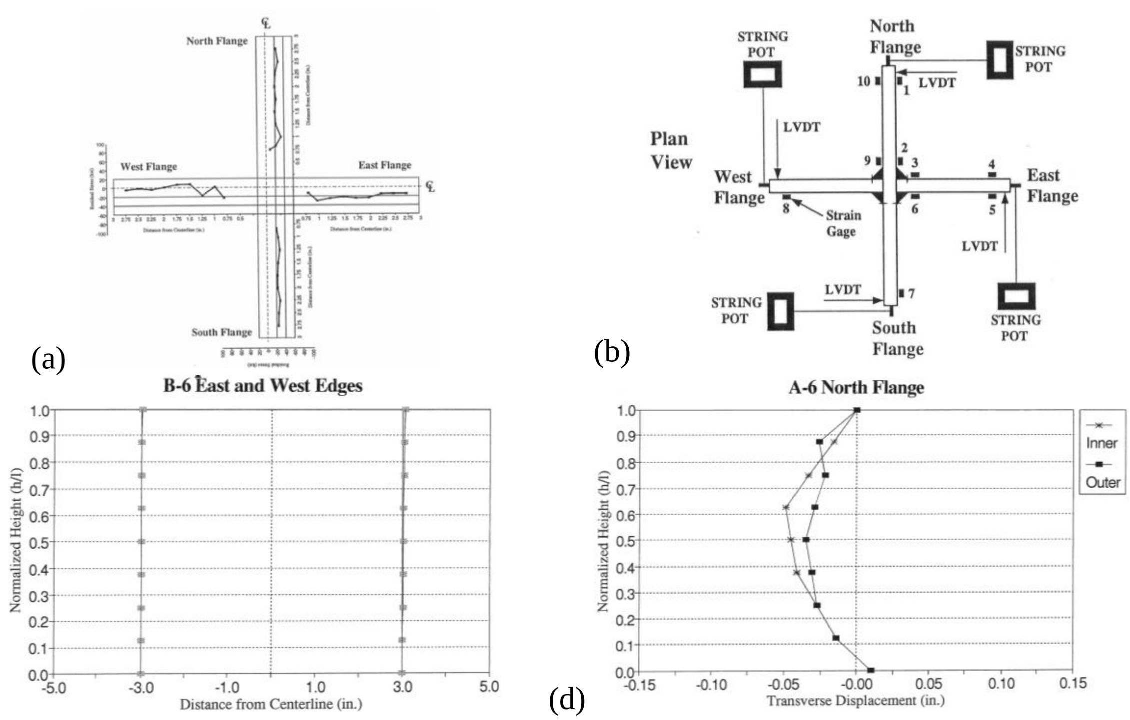

Figure 5: (a) Measured residual stress pattern (specimen B-6), (b) mid-span instrumentation layout, (c) initial sweep displacement measurements (specimen B-6) and (d) initial out-of-flatness displacement measurements (specimen A-6).

The experimental failure loads (P_{Exp}) obtained are given in Table 2, and Figs. 6(a_1)-(a_2) depict the deformed configurations of specimens B-6 and A-9 near collapse – in the latter case, a top view is also shown. As for Fig. 6(b), it displays the normalized load vs. axial shortening (P/P_y *vs.* Δ/Δ_y) equilibrium paths of specimens C-3, C-6 and C-9 (HSLA100), where P_y and Δ_y are the squash load and axial shortening at yield – similar results were obtained for the remaining specimens (Green 2012). The analysis of the experimental results presented prompts the following remarks:

(i) All specimens failed in predominantly torsional modes, exhibiting larger deformations at the central region (but not necessarily exactly at mid-span – note that the failure modes shown in Figs. 6(a_1)-(a_2) are not symmetric: larger deformation above and below mid-span for specimens B-6 and A-9). One possible reason for this asymmetry is the different initial out-of-flatness imperfections exhibited by the four plates forming the cross-section (Green 2012).

(ii) There is a quite satisfactory agreement between the collapse mechanism observed during the tests and the failure mode exhibit by the F_5 column – compare Figs. 6(a_1)-(a_2) with Fig. 3(c). Since the end sections of the two specimens exhibit minute deformations, there is evidence that the actual experimental support conditions are "practically fixed" (but not necessarily equally so).

(iii) All specimens are stub columns, as their axial strength and overall behavior are governed by the (measured) plate material properties. This is confirmed by looking at the P_{Exp}/P_y values in Table 2: all but one are below 1.24 (average of 1.11) – the exception is specimen A-3, which exhibits a 1.65 ratio and, therefore, was excluded from the data bank. This huge discrepancy has to do with the fact that the observed collapse mode did not involve any overall torsional deformations, thus allowing the individual plate longitudinal strains to reach the strain-hardening region (Green 2012).

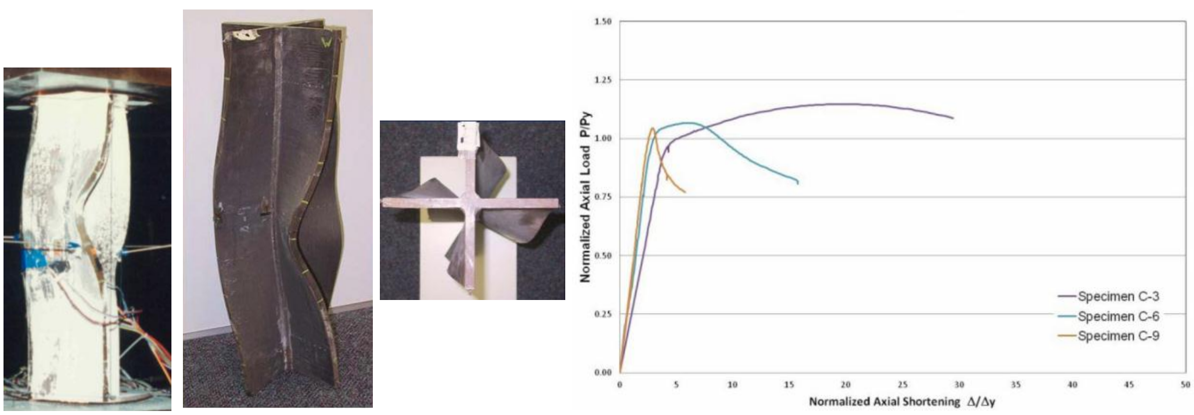

(a_1) (a_2) (b)

Figure 6: (a) Torsional failure modes exhibited by specimens (a_1) B-6 (side view) and (a_2) A-9 (side and top views), and (b) normalized load vs. axial shortening curves concerning specimens C-3, C-6 and C-9.

3.3 Additional Test Results Reported in the Literature

The experimental results collected from the literature concern (i) 5 columns tested by Nishimo *et al.* (1968), with leg width b varying from 77 to 199 mm and thickness t=17 mm, (ii) 12 columns tested by McDermott (1969), with b varying from 17 to 62 mm and t=6 mm, and (iii) 6 columns tested by Rasmussen & Hancock (1992), with b varying from 41 to 72 mm and t=6 mm – the last two column sets include repeated test results. Further details about the measured specimen dimensions and steel properties can be found in the above references. Appendix C provides the (i) cross-section geometry (b, t), (ii) length L, (iii) yield stress f_y and (iv) ultimate stress f_U for the 31 specimens tested – including 8 of the 9 tests carried out by Green (2012), already reported in Table 2 (specimen A-3 was excluded).

4. Direct Strength Method (DSM) Design

The current DSM strength/design curves for cold-formed steel columns are defined by "Winter-type" expressions that (i) were calibrated against fairly large numbers of experimental and/or numerical results and (ii) provide safe and accurate ultimate strength estimates associated with local, distortional, global (flexural or flexural-torsional) and local-global interactive failures on the sole basis of elastic critical buckling (f_{crL}, f_{crD}, f_{crE}) and yield stresses. In the context of this investigation on cruciform columns, which are not (yet) pre-qualified for using the DSM design approach, the relevant nominal strengths are f_{NL} (local/torsional[3]), f_{NE} (global) and f_{NLE} (local-global) (*e.g.*, Schafer 2008).

4.1 Assessment of the Current DSM Ultimate Load Estimates

Fig. 7(a) shows the variation of the ultimate stress ratio f_U/f_y with the critical slenderness λ_T for (i) the test results gathered in this work (see Appendix C) and (ii) also includes the test data obtained by Ratcliffe, taken (scanned) from Chen & Trahair (1994). On the other hand, Fig. 7(b) shows the same variation for the pin-ended and fixed-ended columns analyzed numerically (see Appendices A and B). Finally, Fig. 8 provides the variations of f_U/f_{NL} (Fig. 8(a)), f_U/f_{NE} (Fig. 8(b)) and f_U/f_{NLE} (Fig. 8(c)) with λ_T, including jointly the numerical (P and F columns) and experimental values (white and black circles, respectively) – the associated averages, standard deviations, maximum and minimum values are given in Table 3. The observation analysis of the results displayed in these figures prompts the following remarks:

(i) Since practically all available experimental ultimate loads concern fairly stocky columns (λ_L<1.05 – only two specimens tested by Ratcliffe exhibit higher critical slenderness, but both below 1.5), they

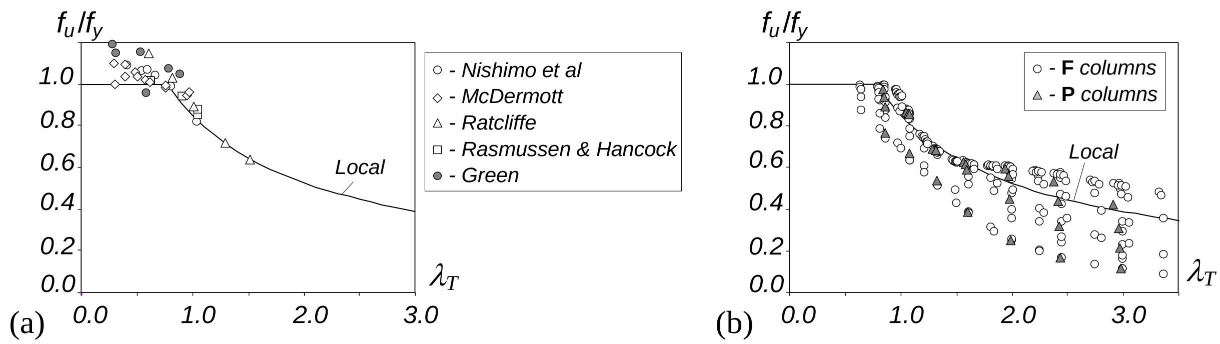

Figure 7: Variation of f_U/f_y with λ_T: (a) experimental tests, (b) P and F columns (numerical).

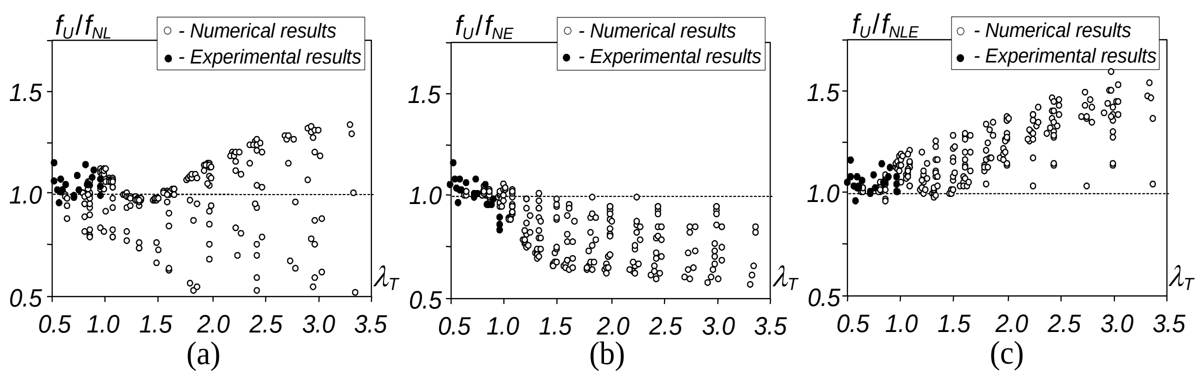

Figure 8: Variation of the experimental and numerical (a) f_U/f_{NL}, (b) f_U/f_{NE} and (c) f_U/f_{NLE} values with λ_T.

[3] Although the two designations are often used indistinctly, due to the fact that local (plate) and torsional deformations are akin in cruciform columns, the authors believe that they are not the same – this work deals with torsional strength and failure.

Table 3: Means and standard deviations of the DSM ultimate strength estimates (experimental and numerical results)

	Experimental			*Numerical (P)*			*Numerical (F)*		
	f_U/f_{NL}	f_U/f_{NE}	f_U/f_{NLE}	f_U/f_{NL}	f_U/f_{NE}	f_U/f_{NLE}	f_U/f_{NL}	f_U/f_{NE}	f_U/f_{NLE}
Mean	*1.06*	*1.03*	*1.07*	*0.87*	*0.85*	*1.16*	*0.96*	*0.82*	*1.18*
Sd. Dev.	*0.06*	*0.09*	*0.06*	*0.23*	*0.13*	*0.10*	*0.23*	*0.14*	*0.15*
Max	*1.24*	*1.24*	*1.24*	*1.15*	*1.02*	*1.32*	*1.38*	*1.05*	*1.58*
Min	*0.95*	*0.83*	*0.96*	*0.29*	*0.60*	*0.99*	*0.25*	*0.51*	*0.96*

are naturally fairly closely predicted (almost always conservatively) by the three DSM nominal strengths (f_{NL}, f_{NE} and f_{NLE}) and, therefore, cannot be used to assess their absolute or relative merits. These merits must be assessed through the prediction of the numerical ultimate loads, which concern columns that were selected to cover a wide slenderness range.

(ii) The DSM local strength curve provides highly scattered and often very unsafe ultimate load estimates: the f_U/f_{NL} averages, standard deviations and minimum values are equal to 0.87/0.23/0.29 (P columns) and 0.96/0.23/0.25 (F columns).

(iii) The DSM global strength curve yields fairly scattered and practically always unsafe ultimate load estimates: the f_U/f_{NE} averages, standard deviations and minimum values are equal to 0.85/0.13/0.60 (P columns) and 0.82/0.14/0.51 (F columns).

(iv) Although the f_{NLE} values provide safe ultimate load predictions for all the 28 P and 224 F columns analyzed, quite a number of them are too conservative: the f_U/f_{NLE} averages, standard deviations and maximum values are equal to 1.16/0.10/1.32 (P columns) and 1.18/0.15/1.58 (F columns).

(v) The rational explanation for these extremely conservative DSM f_{NLE} ultimate strength estimates was very recently unveiled by Trahair (2012), who derived analytical curves that show the variations, with the corresponding slenderness values, of the torsional and local post-critical strength reserves concerning geometrically perfect simply supported cruciform columns. He showed that the former are higher than the latter, particularly in the moderate-to-large slenderness range. This difference may be even more pronounced in columns with warping-prevented end sections, as those considered in this work, due to the influence of secondary warping effects (neglected by Trahair).

(vi) Therefore, it seems logical to expect the quality of the DSM ultimate strength estimates to improve if the current local strength curve is replaced by a more accurate and rational torsional strength curve – the search for such a curve will be addressed in the next subsection. Moreover, since most of the columns analyzed were found to fail in torsional-fexural interactive modes, the proposed torsional strength curve will then be combined with the current DSM global (flexural) strength curve, thus leading to DSM f_{NTE} ultimate strength estimates.

4.2 Proposal for a Novel DSM Design Approach

The first step involved in this proposed novel DSM design approach for cruciform columns consists of using the numerical failure loads concerning the P and F cruciform columns containing pure torsional (T) initial imperfections (see subsection 2.3), which were found to fail in pure torsional modes (without any hint of flexural deformations), to search for a “Winter-type” torsional strength curve that estimates them as accurately as possible. Note that only part of the above numerical torsional failure loads are given in Table 1 – the remaining ones concern columns with the same geometries and larger yield stresses (to achieve higher slenderness values). The search was made by a “trial-and-error” procedure, taking into account that the current DSM local strength curve provides quite accurate estimates for slenderness values up to about 1.4, and has led to

$$f_{NT}=\begin{cases} f_y & \text{if} \quad \lambda_T \le 0.776 \\ f_y\left(\dfrac{f_{crT}}{f_y}\right)^{0.4}\left[1-0.15\left(\dfrac{f_{crT}}{f_y}\right)^{0.4}\right] & \text{if} \quad 0.776<\lambda_T<1.4 \\ f_y\left(\dfrac{f_{crT}}{f_y}\right)^{0.2}\left[1-0.22\left(\dfrac{f_{crT}}{f_y}\right)^{0.26}\right] & \text{if} \quad \lambda_T \ge 1.4 \end{cases} \quad \text{with} \quad \lambda_T=\sqrt{\frac{f_y}{f_{crT}}} \quad . \quad (1)$$

Fig. 9 compares the proposed torsional strength curve with (i) the current DSM local strength curve and (ii) the numerical column torsional failure loads. It is clear that the proposed curve (i) lies well above the current DSM local curve in the moderate-to-high slenderness range and (ii) fits quite nicely the numerical torsional failure loads – the difference never exceeds 3.5%.

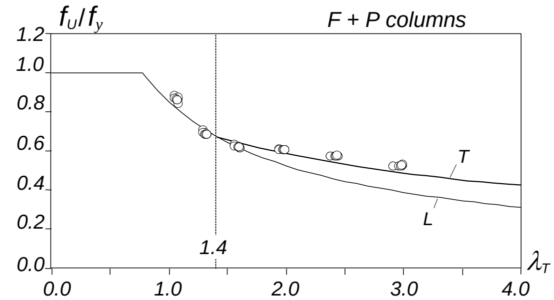

Figure 9: Variation of f_U/f_y with λ_T for the P and F columns.

The next step consists of combining Eq. (1) with the current DSM global strength curve, given by

$$f_{NE}=\begin{cases} f_y\left(0.658^{\lambda_E^2}\right) & \text{if} \quad \lambda_E \le 1.5 \\ f_y\left(\dfrac{0.877}{\lambda_E^2}\right) & \text{if} \quad \lambda_E > 1.5 \end{cases} \quad \text{with} \quad \lambda_E=\sqrt{\frac{f_y}{f_{crE}}} \quad , \quad (2)$$

following a strategy similar to that used to develop design rules against local-global interactive failures. Therefore, it is possible to define a DSM design approach against torsional-flexural column interactive failures, denoted here as "NTE approach", which corresponds to replacing f_y with f_{NE} in Eq. (1) to obtain f_{NTE} ultimate strength estimates. Figs. 10(a)-(b) make it possible to compare the variations, with λ_T, of the f_U/f_{NLE} (Fig. 10(a) – same as Fig. 8(c)) and f_U/f_{NTE} (Fig. 10(b)) ratios, all concerning the numerical (white circles) and experimental (black circles) failure loads. The corresponding averages, standard deviations and maximum/minimum values are also indicated in Figs. 10(a)-(b) – all the values are given in the appendices for the numerical pin-ended columns (Appendix A), numerical fixed-ended columns (Appendix B) and tested specimens (Appendix C). Observations made from these results lead to the following conclusions:

(i) As anticipated, the f_{NTE} ultimate load estimates exhibit higher quality than their f_{NLE} counterparts: the corresponding ultimate-to-predicted stress ratios exhibit (i_1) an average closer to 1.0 (1.09 *vs.* 1.17), (i_2) a smaller standard deviation (0.09 *vs.* 0.15), and (i_3) lower maximum values (1.29 *vs.* 1.58), which are obviously "compensated" by the appearance of a number of more or less relevant underestimations (minimum value 0.92 *vs.* 0.96).

(ii) There are minute quality differences between the numerical ultimate-to-predicted stress ratios concerning the P and F columns, thus indicating that the above remarks apply to both of them.

(iii) Since the available experimental failure loads concern rather stocky columns ($\lambda_T < 1.05$), they are equally well predicted by the two DSM approaches (averages and standard deviations 1.07/0.06).

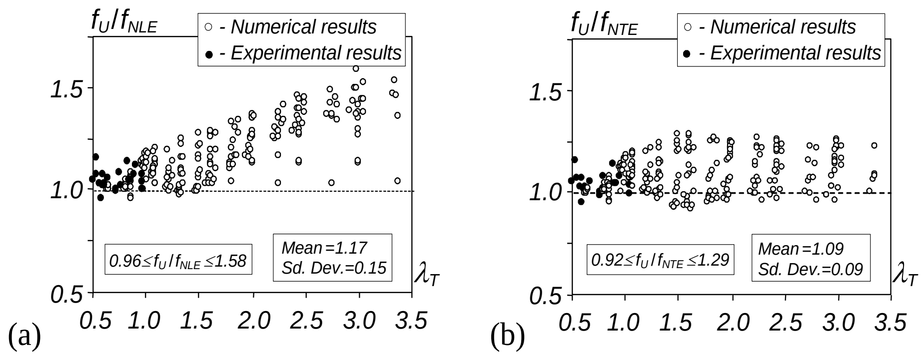

Figure 10: Variation with λ_T of (a) f_U/f_{NLE} and (b) f_U/f_{NTE} for the whole set of tests results and P and F columns.

5. Conclusion

This work presented a numerical and experimental investigation on the behavior (buckling, post-buckling and ultimate strength) and DSM design of short-to-intermediate thin-walled steel equal-leg cruciform pin-ended and fixed-ended columns (the end section secondary warping is prevented in both cases). After addressing the main features of the column buckling and post-buckling behaviors, unveiled through (i) GBT (buckling) and (ii) ABAQUS shell finite element (post-buckling) analyses, the paper provided an overview of an experimental investigation on steel cruciform columns carried out at Lehigh University and recently reported by Green (2012) – it involved 9 specimens with three different lengths, leg widths, and yield strengths. Next, the paper gathered a large column ultimate strength data bank comprising (i) numerical failure loads, concerning 28 pin-ended and 224 fixed-ended initially imperfect columns and covering a wide slenderness range, and (ii) experimental failure loads available in the literature (including the Lehigh tests), almost all of them associated with low slenderness values. This data bank was then used to assess the quality of the estimates provided by the current DSM strength curves for the design against local, global and local-global interactive failures – it was found that the DSM local-global interactive design always provides safe ultimate load predictions, but quite a number of them are excessively conservative (notably in the moderate-to-high slenderness range[4]). On the basis of the above assessment, a novel and more rational DSM design approach is proposed: a new torsional strength curve, developed from numerical (SFEA) results, replaces the current local strength curve – the former lays visibly above the latter in the moderate-to-high slenderness range (the difference increases with the slenderness), thus reflecting the column additional strength. The ensuing DSM-based approach

[4] Since practically all the available experimental results concern rather stocky columns (low slenderness values), it is not surprising that the corresponding ultimate loads are well predicted by the current DSM design curves (even by those associated with local and global failures). Therefore, the assessment was essentially based on the estimates of the numerical failure loads.

against *torsional-flexural failure* is shown to lead to a more efficient (safe and accurate) ultimate strength prediction for the whole set of column failure loads considered in this work: the ultimate-to-predicted stress ratios (f_U/f_{NTE}) are comprised between 0.92 and 1.29, and their average and standard deviations are equal to 1.09 and 0.09, respectively.

References

AISC (American Institute of Steel Construction) (2010). *Specification for Structural Steel Buildings*, ANSI/N360-10, Chicago.

Chen G, Trahair NS (1994). "Inelastic torsional buckling strengths of cruciform columns", *Engineering Structures*, **16**(2), 83-90.

Dabrowsi R (1988). "On torsional stability of cruciform columns", *Journal of Constructional Steel Research*, **9**(1), 51-59.

Dinis P.B., Camotim D. (2006). "On the use of shell finite element analysis to assess the local buckling and post-buckling behaviour of cold-formed steel thin-walled members", *Abstracts of III European Conference on Computational Mechanics: Solids, Structures and Coupled Problems in Engineering* (III ECCM – Lisboa, 5-9/6), 689. (full paper in CD-ROM Proceedings)

Dinis P.B., Camotim D. (2011). "Buckling, post-buckling and strength of cruciform columns", USB Key Drive *Proceedings of SSRC Annual Stability Conference* (Pittsburgh, PA. 10-14/5).

Dinis P.B., Camotim D. (2012). "Post-Buckling Behaviour, Strength and DSM Design of Thin-Walled Cruciform Steel Columns", *Proceedings of Tenth International Conference on Steel Concrete Composite and Hybrid Structures* (ASCCS 2012 – Singapore, 2-4/7), 51-59.

Green P.S. (2012). "Behavior of HPS cruciform columns", USB Key Drive *Proceedings of SSRC Annual Stability Conference*, (Grapevine, TX. 17-21/4).

Hutchinson J., Budiansky B. (1976). "Analytical and numerical study of the effects of initial imperfections on the inelastic buckling of a cruciform column", *Buckling of Structures*, B. Budiansky (ed.), Springer-Verlag, Berlin, 98-105.

Makris N. (2003). "Plastic torsional buckling of cruciform compression members", *Journal of Engineering Mechanics* (ASCE), **129**(6), 689-696.

McDermott, J.F. (1969). "Local Plastic Buckling of A514 Steel Members", *Journal of the Structural Division* (ASCE), **95**(9), 1837-1849.

Nishimo F., Tall L., Okumura T. (1968). "Residual stress and torsional buckling strength of H and cruciform columns", *Transactions of the Japanese Society of Civil Engineers* (JSCE), **160** (December), 57-87.

Rasmussen K.J.R., Hancock G.J. (1992). "Plate slenderness limits for high strength steel sections", *Journal of Constructional Steel Research*, **23**(1-3), 73-96.

Rendall M., Rasmussen K. (2012). "Behaviour of pin-ended flange elements in compression", *Proceedings of Sixth International Conference on Coupled Instabilities in Metal Structures* (CIMS 2012 – Glasgow, 3-5/12), 111-118.

Schafer BW (2008). "Review: the direct strength method of cold-formed steel member design", *Journal of Constructional Steel Research*, **64**(7-8), 766-778.

Schurig M., Bertram, A. (2011). "The torsional buckling of a cruciform column under compressive load with a vertex plasticity model", *International Journal of Solids and Structures*, **48**(1), 1-11.

Simulia Inc. (2008). *Abaqus Standard* (vrs. 6.7-5).

Stowell EZ (1951). *Compressive Strength of Flanges*, National Advisory Committee for Aeronautics (NACA) Report nº 1029.

Trahair N.S. (2012). "Strength design of cruciform steel columns", *Engineering Structures*, **35** (February), 307-313.

Trahair N.S. (2013). "Shear effect on cruciform post-buckling", *Engineering Structures*, **49** (April), 24-26.

Young B. (2004). "Tests and design of fixed-ended cold-formed steel plain angle columns", *Journal of Structural Engineering* (ASCE), **130**(12), 1931-1940.

APPENDIX A

Table A1 – P columns: SFEA ultimate strengths and their DSM estimates (dimensions in mm, stresses in MPa)

				SFEA			DSM									
b	t	L	f_{crE}	f_{crT}	f_y	f_U	λ_T	λ_E	f_{NL}	f_{NE}	f_{NLE}	f_{NTE}	f_U/f_{NL}	f_U/f_{NE}	f_U/f_{NLE}	f_U/f_{NTE}
					150	146	0.84	0.26	143	146	140	140	1.02	1.00	1.04	1.04
					235	204	1.05	0.33	193	225	187	187	1.06	0.91	1.09	1.09
					355	245	1.29	0.40	254	332	243	243	0.97	0.74	1.01	1.01
80	4	1000	2212	212	520	325	1.57	0.48	325	471	305	330	1.00	0.69	1.07	0.99
					800	475	1.94	0.60	429	688	389	455	1.11	0.69	1.22	1.04
					1200	636	2.38	0.74	555	956	481	602	1.15	0.67	1.32	1.06
					1800	762	2.91	0.90	717	1280	578	771	1.06	0.60	1.32	0.99
					150	141	0.85	0.39	141	141	135	135	1.00	1.00	1.04	1.04
					235	202	1.07	0.49	191	213	179	179	1.06	0.95	1.13	1.13
					355	242	1.31	0.60	251	305	227	227	0.96	0.79	1.07	1.07
80	4	1500	983	205	520	321	1.59	0.73	322	417	279	296	1.00	0.77	1.15	1.09
					800	446	1.97	0.90	424	569	341	386	1.05	0.78	1.31	1.16
					1200	523	2.42	1.10	548	720	396	471	0.95	0.73	1.32	1.11
					1800	552	2.96	1.35	708	837	436	535	0.78	0.66	1.27	1.03
					150	134	0.86	0.52	141	134	130	130	0.95	1.00	1.03	1.03
					235	201	1.08	0.65	190	197	169	169	1.06	1.02	1.19	1.19
					355	242	1.32	0.80	250	271	209	209	0.97	0.89	1.16	1.16
80	4	2000	553	203	520	307	1.60	0.97	320	351	248	254	0.96	0.88	1.24	1.21
					800	359	1.99	1.20	422	437	286	307	0.85	0.82	1.26	1.17
					1200	380	2.43	1.47	546	484	306	335	0.70	0.79	1.24	1.13
					1800	386	2.98	1.80	705	485	306	336	0.55	0.80	1.26	1.15
					150	115	0.86	0.78	140	116	116	116	0.82	0.99	0.99	0.99
					235	157	1.08	0.98	190	157	145	145	0.83	1.00	1.08	1.08
					355	190	1.33	1.20	249	194	167	167	0.76	0.98	1.14	1.14
80	4	3000	246	201	520	202	1.61	1.45	319	215	179	166	0.63	0.94	1.13	1.22
					800	202	1.99	1.80	421	216	179	167	0.48	0.94	1.13	1.21
					1200	202	2.44	2.21	545	216	179	167	0.37	0.94	1.13	1.21
					1800	202	2.99	2.71	703	216	179	167	0.29	0.94	1.13	1.21
												Mean	0.87	0.85	1.16	1.10
												Sd. Deviation	0.23	0.13	0.10	0.08
												Max	1.15	1.02	1.32	0.99
												Min	0.29	0.60	0.99	1.22

APPENDIX B

Table B1 – F columns: SFEA ultimate strengths and their DSM estimates (dimensions in mm, stresses in MPa)

				SFEA			DSM									
b	t	L	f_{crE}	f_{crT}	f_y	f_U	λ_T	λ_E	f_{NL}	f_{NE}	f_{NLE}	f_{NTE}	f_U/f_{NL}	f_U/f_{NE}	f_U/f_{NLE}	f_U/f_{NTE}
					150	149	0.84	0.13	143	149	142	142	1.04	1.00	1.05	1.05
					235	207	1.05	0.16	193	232	192	192	1.07	0.89	1.08	1.08
					355	250	1.29	0.20	254	349	251	251	0.99	0.72	1.00	1.00
80	4	1000	8849	212	520	330	1.57	0.24	325	507	320	351	1.01	0.65	1.03	0.94
					800	488	1.94	0.30	429	770	419	502	1.14	0.63	1.17	0.97
					1200	688	2.38	0.37	555	1134	535	696	1.24	0.61	1.28	0.99
					1800	942	2.91	0.45	717	1653	679	955	1.31	0.57	1.39	0.99
					150	149	0.85	0.20	141	148	140	140	1.06	1.01	1.07	1.07
					235	204	1.07	0.24	191	229	188	188	1.07	0.89	1.09	1.09
					355	245	1.31	0.30	251	342	245	245	0.98	0.72	1.00	1.00
80	4	1500	3933	205	520	325	1.59	0.36	322	492	310	341	1.01	0.66	1.05	0.95
					800	485	1.97	0.45	424	735	401	479	1.14	0.66	1.21	1.01
					1200	688	2.42	0.55	548	1056	506	652	1.25	0.65	1.36	1.06
					1800	940	2.96	0.68	708	1486	628	869	1.33	0.63	1.50	1.08
					150	149	0.86	0.26	141	146	138	138	1.06	1.02	1.08	1.08
					235	203	1.08	0.33	190	225	185	185	1.07	0.90	1.10	1.10
					355	242	1.32	0.40	250	332	239	239	0.97	0.73	1.01	1.01
80	4	2000	2212	203	520	322	1.60	0.48	320	471	300	328	1.01	0.68	1.07	0.98
					800	483	1.99	0.60	422	688	383	452	1.14	0.70	1.26	1.07
					1200	689	2.43	0.74	546	956	473	598	1.26	0.72	1.46	1.15
					1800	900	2.98	0.90	705	1280	569	765	1.28	0.70	1.58	1.18
					150	139	0.86	0.39	140	141	134	134	0.99	0.99	1.03	1.03
					235	202	1.08	0.49	190	213	178	178	1.06	0.95	1.14	1.14
					355	242	1.33	0.60	249	305	226	226	0.97	0.79	1.07	1.07
80	4	3000	983	201	520	321	1.61	0.73	319	417	277	295	1.01	0.77	1.16	1.09
					800	458	1.99	0.90	421	569	338	385	1.09	0.80	1.35	1.19
					1200	566	2.44	1.10	545	720	394	470	1.04	0.79	1.44	1.20
					1800	610	2.99	1.35	703	837	433	534	0.87	0.73	1.41	1.14
					150	137	0.86	0.52	140	134	130	130	0.98	1.02	1.06	1.06
					235	202	1.08	0.65	190	197	168	168	1.07	1.03	1.20	1.20
					355	242	1.33	0.80	249	271	209	209	0.97	0.89	1.16	1.16
80	4	4000	553	201	520	316	1.61	0.97	319	351	247	254	0.99	0.90	1.28	1.24
					800	383	1.99	1.20	421	437	285	307	0.91	0.88	1.34	1.25
					1200	408	2.44	1.47	544	484	305	335	0.75	0.84	1.34	1.22
					1800	412	2.99	1.80	702	485	305	336	0.59	0.85	1.35	1.23
					150	126	0.86	0.65	140	126	124	124	0.90	1.00	1.01	1.01
					235	176	1.08	0.81	190	178	157	157	0.93	0.99	1.12	1.12
					355	235	1.33	1.00	249	233	189	189	0.94	1.01	1.25	1.25
80	4	5000	354	201	520	269	1.61	1.21	319	281	214	210	0.84	0.96	1.26	1.28
					800	286	2.00	1.50	421	310	228	229	0.68	0.92	1.25	1.25
					1200	288	2.44	1.84	544	310	228	229	0.53	0.93	1.26	1.26
					1800	288	2.99	2.26	702	310	228	229	0.41	0.93	1.26	1.26

Table B2 – F columns: SFEA ultimate strengths and their DSM estimates (dimensions in mm, stresses in MPa)

				SFEA			DSM									
b	t	L	f_{crE}	f_{crT}	f_y	f_U	λ_T	λ_E	f_{NL}	f_{NE}	f_{NLE}	f_{NTE}	f_U/f_{NL}	f_U/f_{NE}	f_U/f_{NLE}	f_U/f_{NTE}
80	4	6000	246	201	150	112	0.86	0.78	140	116	116	116	0.80	0.96	0.96	0.96
					235	149	1.08	0.98	190	157	145	145	0.79	0.95	1.03	1.03
					355	182	1.33	1.20	249	194	167	167	0.73	0.94	1.09	1.09
					520	201	1.61	1.45	319	215	178	166	0.63	0.94	1.13	1.21
					800	203	2.00	1.80	421	216	179	167	0.48	0.94	1.13	1.22
					1200	203	2.44	2.21	544	216	179	167	0.37	0.94	1.13	1.22
					1800	203	2.99	2.71	702	216	179	167	0.29	0.94	1.13	1.22
90	4	1500	4977	164	150	146	0.96	0.17	131	148	130	130	1.11	0.99	1.12	1.12
					235	176	1.20	0.22	177	230	175	175	0.99	0.76	1.01	1.01
					355	225	1.47	0.27	232	345	227	243	0.97	0.65	0.99	0.93
					520	317	1.78	0.32	297	498	288	333	1.07	0.64	1.10	0.95
					800	468	2.21	0.40	390	748	374	470	1.20	0.63	1.25	1.00
					1200	646	2.71	0.49	504	1085	473	643	1.28	0.60	1.37	1.00
					1800	870	3.32	0.60	650	1547	591	866	1.34	0.56	1.47	1.00
90	4	2000	2799	161	150	146	0.96	0.23	131	147	129	129	1.12	1.00	1.14	1.14
					235	175	1.21	0.29	176	227	172	172	0.99	0.77	1.02	1.02
					355	225	1.48	0.36	231	337	223	238	0.98	0.67	1.01	0.95
					520	316	1.80	0.43	295	481	281	323	1.07	0.66	1.13	0.98
					800	464	2.23	0.53	388	710	360	449	1.20	0.65	1.29	1.03
					1200	635	2.73	0.65	502	1003	448	601	1.27	0.63	1.42	1.06
					1800	835	3.34	0.80	647	1375	546	783	1.29	0.61	1.53	1.07
90	4	3000	1244	160	150	144	0.97	0.35	130	143	126	126	1.11	1.01	1.14	1.14
					235	175	1.21	0.43	175	217	167	167	1.00	0.81	1.05	1.05
					355	225	1.49	0.53	230	315	213	224	0.98	0.71	1.06	1.00
					520	316	1.80	0.65	294	437	263	297	1.08	0.72	1.20	1.07
					800	448	2.24	0.80	387	611	326	395	1.16	0.73	1.37	1.13
					1200	574	2.74	0.98	500	801	387	496	1.15	0.72	1.48	1.16
					1800	644	3.36	1.20	644	982	441	589	1.00	0.66	1.46	1.09
90	4	5000	448	159	150	133	0.97	0.58	130	130	118	118	1.02	1.02	1.12	1.12
					235	163	1.22	0.72	175	189	152	152	0.93	0.86	1.08	1.08
					355	224	1.49	0.89	229	255	185	187	0.98	0.88	1.21	1.20
					520	285	1.81	1.08	293	320	214	227	0.97	0.89	1.33	1.25
					800	323	2.24	1.34	386	379	239	263	0.84	0.85	1.35	1.23
					1200	333	2.75	1.64	499	393	245	271	0.67	0.85	1.36	1.23
					1800	333	3.36	2.00	643	393	245	271	0.52	0.85	1.36	1.23
90	4	7000	229	159	150	108	0.97	0.81	130	114	108	108	0.83	0.95	1.00	1.00
					235	143	1.22	1.01	175	153	132	132	0.82	0.94	1.09	1.09
					355	175	1.49	1.25	229	185	150	142	0.76	0.94	1.17	1.23
					520	164	1.81	1.51	293	200	158	152	0.56	0.82	1.04	1.08
					800	163	2.24	1.87	386	200	158	152	0.42	0.81	1.03	1.07
					1200	163	2.75	2.29	499	200	158	152	0.33	0.81	1.03	1.07
					1800	164	3.36	2.81	643	200	158	152	0.25	0.82	1.04	1.08

Table B3 – F columns: SFEA ultimate strengths and their DSM estimates (dimensions in mm, stresses in MPa)

				SFEA			DSM									
b	t	L	f_{crE}	f_{crT}	f_y	f_U	λ_T	λ_E	f_{NL}	f_{NE}	f_{NLE}	f_{NTE}	f_U/f_{NL}	f_U/f_{NE}	f_U/f_{NLE}	f_U/f_{NTE}
					150	148	0.85	0.17	141	148	140	140	1.05	1.00	1.06	1.06
					235	203	1.07	0.22	191	230	189	189	1.06	0.88	1.07	1.07
					355	243	1.31	0.27	251	345	247	247	0.97	0.71	0.99	0.99
120	6	2000	4977	207	520	323	1.59	0.32	322	498	313	344	1.00	0.65	1.03	0.94
					800	483	1.97	0.40	425	748	407	487	1.14	0.65	1.19	0.99
					1200	679	2.41	0.49	550	1085	516	667	1.24	0.63	1.32	1.02
					1800	925	2.95	0.60	710	1547	645	900	1.30	0.60	1.43	1.03
					150	146	0.86	0.26	141	146	138	138	1.04	1.00	1.06	1.06
					235	203	1.08	0.33	190	225	185	185	1.07	0.90	1.10	1.10
					355	243	1.32	0.40	250	332	239	239	0.97	0.73	1.02	1.02
120	6	3000	2212	203	520	321	1.60	0.48	320	471	300	328	1.00	0.68	1.07	0.98
					800	478	1.99	0.60	422	688	383	452	1.13	0.70	1.25	1.06
					1200	659	2.43	0.74	546	956	473	598	1.21	0.69	1.39	1.10
					1800	849	2.98	0.90	705	1280	569	765	1.20	0.66	1.49	1.11
					150	141	0.86	0.43	140	139	133	133	1.01	1.02	1.06	1.06
					235	196	1.08	0.54	190	208	175	175	1.03	0.94	1.12	1.12
					355	243	1.33	0.67	249	295	220	220	0.98	0.82	1.10	1.10
120	6	5000	796	201	520	320	1.61	0.81	319	396	267	282	1.00	0.81	1.20	1.14
					800	438	1.99	1.00	421	525	321	359	1.04	0.83	1.36	1.22
					1200	509	2.44	1.23	544	639	364	424	0.94	0.80	1.40	1.20
					1800	530	2.99	1.50	703	698	386	458	0.75	0.76	1.37	1.16
					150	131	0.86	0.61	140	129	126	126	0.93	1.02	1.04	1.04
					235	185	1.08	0.76	190	184	161	161	0.98	1.00	1.15	1.15
					355	239	1.33	0.93	249	246	196	196	0.96	0.97	1.22	1.22
120	6	7000	406	201	520	289	1.61	1.13	319	304	225	225	0.91	0.95	1.28	1.29
					800	317	2.00	1.40	421	351	247	254	0.75	0.90	1.28	1.25
					1200	323	2.44	1.72	544	356	250	258	0.59	0.91	1.29	1.25
					1800	323	2.99	2.10	702	356	250	258	0.46	0.91	1.29	1.25
					150	111	0.86	0.78	140	116	116	116	0.79	0.96	0.96	0.96
					235	149	1.08	0.98	190	157	145	145	0.79	0.95	1.03	1.03
					355	182	1.33	1.20	249	194	167	167	0.73	0.94	1.09	1.09
120	6	9000	246	201	520	200	1.61	1.45	319	215	178	166	0.63	0.93	1.12	1.21
					800	204	2.00	1.80	421	216	179	167	0.49	0.95	1.14	1.22
					1200	204	2.44	2.21	544	216	179	167	0.37	0.95	1.14	1.22
					1800	204	2.99	2.71	702	216	179	167	0.29	0.95	1.14	1.22
					150	131	1.05	0.14	123	149	122	122	1.06	0.88	1.07	1.07
					235	160	1.32	0.17	166	232	164	164	0.97	0.69	0.97	0.97
					355	220	1.62	0.21	217	348	214	239	1.02	0.63	1.03	0.92
150	6	2000	7775	135	520	314	1.96	0.26	277	506	272	328	1.13	0.62	1.16	0.96
					800	451	2.43	0.32	364	766	354	466	1.24	0.59	1.27	0.97
					1200	616	2.98	0.39	470	1125	451	643	1.31	0.55	1.37	0.96
					1800	835	3.65	0.48	605	1634	569	878	1.38	0.51	1.47	0.95

Table B4 – F columns: SFEA ultimate strengths and their DSM estimates (dimensions in mm, stresses in MPa)

				SFEA			DSM									
b	t	L	f_{crE}	f_{crT}	f_y	f_U	λ_T	λ_E	f_{NL}	f_{NE}	f_{NLE}	f_{NTE}	f_U/f_{NL}	f_U/f_{NE}	f_U/f_{NLE}	f_U/f_{NTE}
150	6	3000	3456	131	150	130	1.07	0.21	122	147	121	121	1.07	0.88	1.08	1.08
					235	159	1.34	0.26	164	228	161	161	0.97	0.70	0.99	0.99
					355	219	1.64	0.32	214	340	209	233	1.02	0.64	1.05	0.94
					520	313	1.99	0.39	274	488	263	317	1.14	0.64	1.19	0.99
					800	448	2.47	0.48	360	726	339	443	1.24	0.62	1.32	1.01
					1200	609	3.02	0.59	465	1038	424	598	1.31	0.59	1.44	1.02
					1800	803	3.70	0.72	598	1447	522	790	1.34	0.55	1.54	1.02
150	6	5000	1244	130	150	131	1.08	0.35	121	143	117	117	1.08	0.92	1.12	1.12
					235	159	1.35	0.43	163	217	155	155	0.97	0.73	1.03	1.03
					355	218	1.66	0.53	213	315	198	218	1.02	0.69	1.10	1.00
					520	308	2.00	0.65	273	437	244	287	1.13	0.71	1.26	1.07
					800	429	2.49	0.80	358	611	302	382	1.20	0.70	1.42	1.12
					1200	545	3.04	0.98	462	801	359	480	1.18	0.68	1.52	1.13
					1800	606	3.73	1.20	595	982	408	570	1.02	0.62	1.49	1.06
150	6	7000	635	129	150	125	1.08	0.49	121	136	114	114	1.03	0.92	1.10	1.10
					235	159	1.35	0.61	163	201	147	147	0.97	0.79	1.08	1.08
					355	218	1.66	0.75	213	281	183	197	1.02	0.78	1.19	1.11
					520	294	2.01	0.91	272	369	219	249	1.08	0.80	1.35	1.18
					800	370	2.49	1.12	358	472	256	307	1.03	0.78	1.45	1.21
					1200	404	3.05	1.37	462	544	280	346	0.88	0.74	1.44	1.17
					1800	408	3.73	1.68	595	557	284	353	0.69	0.73	1.44	1.16
150	6	9000	384	129	150	129	1.08	0.63	121	127	109	109	1.06	1.01	1.19	1.19
					235	159	1.35	0.78	163	182	138	138	0.98	0.87	1.15	1.15
					355	211	1.66	0.96	213	241	166	173	0.99	0.88	1.27	1.22
					520	256	2.01	1.16	272	295	189	206	0.94	0.87	1.35	1.24
					800	283	2.49	1.44	358	334	205	229	0.79	0.85	1.38	1.24
					1200	283	3.05	1.77	461	337	206	230	0.61	0.84	1.37	1.23
					1800	283	3.74	2.17	594	337	206	230	0.48	0.84	1.37	1.23
120	8	1500	8853	375	150	149	0.63	0.13	150	149	149	149	0.99	1.00	1.00	1.00
					235	233	0.79	0.16	232	232	230	230	1.00	1.00	1.01	1.01
					355	337	0.97	0.20	307	349	304	304	1.10	0.97	1.11	1.11
					520	395	1.18	0.24	396	507	390	390	1.00	0.78	1.01	1.01
					800	510	1.46	0.30	525	770	513	545	0.97	0.66	0.99	0.94
					1200	735	1.79	0.37	683	1134	658	759	1.08	0.65	1.12	0.97
					1800	1050	2.19	0.45	884	1653	838	1045	1.19	0.64	1.25	1.00
120	8	2000	4980	365	150	148	0.64	0.17	150	148	148	148	0.99	1.00	1.00	1.00
					235	232	0.80	0.22	230	230	227	227	1.01	1.01	1.02	1.02
					355	338	0.99	0.27	305	345	299	299	1.11	0.98	1.13	1.13
					520	390	1.19	0.32	393	498	382	382	0.99	0.78	1.02	1.02
					800	505	1.48	0.40	521	748	498	530	0.97	0.68	1.01	0.95
					1200	731	1.81	0.49	676	1085	634	728	1.08	0.67	1.15	1.00
					1800	1040	2.22	0.60	876	1547	796	984	1.19	0.67	1.31	1.06

Table B5 – F columns: SFEA ultimate strengths and their DSM estimates (dimensions in mm, stresses in MPa)

				SFEA			DSM									
b	t	L	f_{crE}	f_{crT}	f_y	f_U	λ_T	λ_E	f_{NL}	f_{NE}	f_{NLE}	f_{NTE}	f_U/f_{NL}	f_U/f_{NE}	f_U/f_{NLE}	f_U/f_{NTE}
					150	146	0.65	0.26	150	146	146	146	0.97	1.00	1.00	1.00
					235	228	0.81	0.33	229	225	222	222	1.00	1.01	1.03	1.03
					355	339	0.99	0.40	303	332	289	289	1.12	1.02	1.17	1.17
120	8	3000	2213	359	520	388	1.20	0.48	390	471	366	366	0.99	0.82	1.06	1.06
					800	503	1.49	0.60	517	688	469	492	0.97	0.73	1.07	1.02
					1200	721	1.83	0.74	672	956	581	652	1.07	0.75	1.24	1.11
					1800	964	2.24	0.90	870	1281	700	836	1.11	0.75	1.38	1.15
					150	141	0.65	0.43	150	139	139	139	0.94	1.02	1.02	1.02
					235	217	0.81	0.54	228	208	208	208	0.95	1.04	1.04	1.04
					355	309	1.00	0.67	302	295	266	266	1.02	1.05	1.16	1.16
120	8	5000	797	356	520	389	1.21	0.81	389	396	325	325	1.00	0.98	1.20	1.20
					800	500	1.50	1.00	516	526	392	389	0.97	0.95	1.28	1.28
					1200	582	1.84	1.23	670	639	446	461	0.87	0.91	1.31	1.26
					1800	609	2.25	1.50	867	699	472	498	0.70	0.87	1.29	1.22
					150	131	0.65	0.61	150	129	129	129	0.87	1.02	1.02	1.02
					235	185	0.81	0.76	228	184	184	184	0.81	1.00	1.00	1.00
					355	246	1.00	0.93	302	246	236	236	0.81	1.00	1.04	1.04
120	8	7000	407	356	520	299	1.21	1.13	389	304	272	272	0.77	0.98	1.10	1.10
					800	343	1.50	1.40	516	351	300	274	0.67	0.98	1.14	1.25
					1200	354	1.84	1.72	670	357	303	278	0.53	0.99	1.17	1.27
					1800	354	2.25	2.10	867	357	303	278	0.41	0.99	1.17	1.27
					150	148	0.79	0.14	148	149	147	147	1.00	0.99	1.00	1.00
					235	220	0.99	0.17	201	232	199	199	1.09	0.95	1.10	1.10
					355	260	1.22	0.21	264	348	261	261	0.98	0.75	1.00	1.00
150	8	2000	7778	239	520	330	1.47	0.26	339	506	333	357	0.97	0.65	0.99	0.93
					800	488	1.83	0.32	448	766	436	508	1.09	0.64	1.12	0.96
					1200	699	2.24	0.39	580	1125	557	704	1.21	0.62	1.26	0.99
					1800	963	2.74	0.48	749	1634	705	964	1.29	0.59	1.37	1.00
					150	147	0.80	0.21	147	147	145	145	1.00	1.00	1.01	1.01
					235	221	1.01	0.26	199	228	195	195	1.11	0.97	1.13	1.13
					355	257	1.24	0.32	262	340	254	254	0.98	0.76	1.01	1.01
150	8	3000	3457	233	520	327	1.50	0.39	336	488	322	345	0.97	0.67	1.01	0.95
					800	485	1.85	0.48	443	726	417	484	1.09	0.67	1.16	1.00
					1200	690	2.27	0.59	574	1038	523	655	1.20	0.66	1.32	1.05
					1800	934	2.78	0.72	741	1448	646	867	1.26	0.65	1.45	1.08
					150	144	0.81	0.35	146	143	141	141	0.99	1.01	1.02	1.02
					235	222	1.01	0.43	198	217	188	188	1.12	1.02	1.18	1.18
					355	257	1.24	0.53	261	315	241	241	0.99	0.82	1.07	1.07
150	8	5000	1245	229	520	327	1.51	0.65	334	437	298	312	0.98	0.75	1.10	1.05
					800	475	1.87	0.80	441	611	371	417	1.08	0.78	1.28	1.14
					1200	623	2.29	0.98	571	801	442	525	1.09	0.78	1.41	1.19
					1800	710	2.80	1.20	738	983	503	624	0.96	0.72	1.41	1.14

Table B6 - F columns: SFEA ultimate strengths and their DSM estimates (dimensions in mm, stresses in MPa)

				SFEA			DSM									
b	t	L	f_{crE}	f_{crT}	f_y	f_U	λ_T	λ_E	f_{NL}	f_{NE}	f_{NLE}	f_{NTE}	f_U/f_{NL}	f_U/f_{NE}	f_U/f_{NLE}	f_U/f_{NTE}
150	8	7000	635	229	150	139	0.81	0.49	146	136	136	136	0.95	1.02	1.02	1.02
					235	209	1.01	0.61	198	201	178	178	1.06	1.04	1.17	1.17
					355	253	1.25	0.75	260	281	223	223	0.97	0.90	1.13	1.13
					520	327	1.51	0.90	334	369	267	270	0.98	0.89	1.22	1.21
					800	419	1.87	1.12	441	472	314	334	0.95	0.89	1.34	1.25
					1200	460	2.29	1.37	570	544	344	377	0.81	0.85	1.34	1.22
					1800	468	2.81	1.68	737	557	349	385	0.64	0.84	1.34	1.22
150	8	9000	384	228	150	129	0.81	0.62	146	127	127	127	0.88	1.01	1.01	1.01
					235	181	1.01	0.78	198	182	167	167	0.91	1.00	1.09	1.09
					355	245	1.25	0.96	260	241	201	201	0.94	1.02	1.22	1.22
					520	241	1.51	1.16	334	295	230	223	0.72	0.82	1.05	1.08
					800	241	1.87	1.44	441	335	250	248	0.55	0.72	0.96	0.97
					1200	241	2.29	1.77	570	337	251	250	0.42	0.72	0.96	0.97
					1800	241	2.81	2.16	736	337	251	250	0.33	0.72	0.96	0.97
												Mean	0.96	0.82	1.18	1.09
												Sd. Deviation	0.23	0.14	0.15	0.10
												Max	1.38	1.05	1.58	1.29
												Min	0.25	0.51	0.96	0.92

APPENDIX C

Table C1 – Column experimental ultimate stresses and their DSM estimates (dimensions in mm, stresses in MPa)

							FEA						DSM				
	b	t	L	f_{crE}	f_{crT}	f_y	f_U	λ_T	λ_E	f_{NL}	f_{NE}	f_{NLE}	f_{NTE}	f_U/f_{NL}	f_U/f_{NE}	f_U/f_{NLE}	f_U/f_{NTE}
Nishimo *et al.* (1968)	77.0	17.1	600.0	23006	4282	735	801	0.41	0.18	735	725	725	725	1.09	1.10	1.10	1.10
	103.0	17.2	801.0	22993	2476	735	779	0.54	0.18	735	725	725	725	1.06	1.07	1.07	1.07
	127.0	17.2	1000.0	22381	1643	735	764	0.67	0.18	735	724	724	724	1.04	1.05	1.05	1.05
	154.0	17.2	1200.0	22824	1130	735	727	0.81	0.18	717	725	711	711	1.01	1.00	1.02	1.02
	199.0	17.3	1600.0	21413	677	735	602	1.04	0.19	608	724	602	602	0.99	0.83	1.00	1.00
McDermott (1969)	17.2	6.2	114.3	32452	8608	752	827	0.30	0.15	752	744	744	744	1.10	1.11	1.11	1.11
	17.7	6.3	152.4	19118	8436	752	752	0.30	0.20	752	739	739	739	1.00	1.02	1.02	1.02
	23.8	6.3	152.4	34301	4965	752	821	0.39	0.15	752	745	745	745	1.09	1.10	1.10	1.10
	24.3	6.3	203.2	20074	4763	752	779	0.40	0.19	752	740	740	740	1.04	1.05	1.05	1.05
	30.2	6.3	190.5	35291	3203	752	793	0.48	0.15	752	745	745	745	1.06	1.06	1.06	1.06
	30.8	6.2	253.5	20697	2975	752	779	0.50	0.19	752	740	740	740	1.04	1.05	1.05	1.05
	36.2	6.3	229.1	34890	2279	752	765	0.57	0.15	752	745	745	745	1.02	1.03	1.03	1.03
	37.1	6.1	304.8	20678	1998	752	758	0.61	0.19	752	740	740	740	1.01	1.02	1.02	1.02
	48.9	6.4	304.8	35867	1312	752	738	0.76	0.14	752	745	745	745	0.98	0.99	0.99	0.99
	48.6	6.4	405.6	19980	1306	752	745	0.76	0.19	752	740	740	740	0.99	1.01	1.01	1.01
	61.7	6.4	381.0	36527	838	752	710	0.95	0.14	662	745	658	658	1.07	0.95	1.08	1.08
	61.7	6.3	508.0	20545	799	752	724	0.97	0.19	652	740	645	645	1.11	0.98	1.12	1.12
Rasmussen & Hancock (1992)	41.0	5.9	300.0	26629	1884	740	750	0.63	0.17	740	731	731	731	1.01	1.03	1.03	1.03
	41.0	6.0	300.0	26631	1903	740	751	0.62	0.17	740	731	731	731	1.01	1.03	1.03	1.03
	56.0	5.4	400.0	27272	886	740	694	0.91	0.16	667	732	662	662	1.04	0.95	1.05	1.05
	55.0	5.4	400.0	26548	898	740	695	0.91	0.17	670	731	665	665	1.04	0.95	1.05	1.05
	72.0	5.9	450.0	35156	675	740	629	1.05	0.15	610	734	607	607	1.03	0.86	1.04	1.04
	71.0	5.9	450.0	34764	675	740	650	1.05	0.15	610	733	606	606	1.07	0.89	1.07	1.07
Green (2012)	38.1	12.7	228.6	39457	7576	600	714	0.28	0.12	600	596	596	596	1.19	1.20	1.20	1.20
	38.1	12.7	228.6	39457	7592	758	870	0.32	0.14	758	752	752	752	1.15	1.16	1.16	1.16
	76.2	12.7	457.2	38810	2094	331	410	0.40	0.09	331	330	330	330	1.24	1.24	1.24	1.24
	76.2	12.7	457.2	38810	2101	600	690	0.53	0.12	600	596	596	596	1.15	1.16	1.16	1.16
	76.2	12.7	457.2	38810	2105	758	809	0.60	0.14	758	752	752	752	1.07	1.08	1.08	1.08
	114.3	12.7	685.8	38677	962	331	316	0.59	0.09	331	330	330	330	0.95	0.96	0.96	0.96
	114.3	12.7	685.8	38677	965	600	642	0.79	0.12	594	596	591	591	1.08	1.08	1.09	1.09
	114.3	12.7	685.8	38677	967	758	792	0.89	0.14	698	752	694	694	1.14	1.05	1.14	1.14
													Mean	1.06	1.03	1.07	1.07
													Sd. Deviation	0.06	0.09	0.06	0.06
													Max.	1.24	1.24	1.24	1.24
													Min.	0.95	0.83	0.96	0.96